Influence of Vortices in the Sinus of Valsalva on Local Wall Shear Stress Distribution

Tomohiro Fukui[*1], Koji Morinishi[2]

Department of Mechanical and System Engineering, Kyoto Institute of Technology
Matsugasaki Goshokaido-cho, Sakyo-ku, Kyoto, 606-8585, Japan

[*1]fukui@kit.ac.jp; [2]morinisi@kit.ac.jp

Abstract- **Transposition of the great arteries (TGA) is one of the most severe congenital heart diseases. The arterial switch operation (ASO) is the procedure of preference for treatment of TGA. After ASO, some patients suffer from circulatory system problems such as neo-aortic root dilatation and neo-aortic valve regurgitation, and supravalvar pulmonary stenosis. The neo-aortic root dilatation is often explained by the structural vascular difference between normal great arteries and the neo-aorta after ASO. Since the aortic and pulmonary roots generally remain in situ after ASO, i.e., the original pulmonary artery is connected to the left ventricle (LV), whereas the original aorta is connected to the right ventricle, the neo-aorta has no sinus of Valsalva after ASO. The influence of these morphological changes on the blood flow field at the aortic root should be investigated in detail as well as the structural vascular difference to consider the circular system problems. In this study, we apply the virtual flux method (VFM), which is a tool to describe stationary or moving body shapes in a Cartesian grid, to the 2D aortic valves and reproduce the blood flow fields around the aortic valves and the sinus of Valsalva by regularized lattice Boltzmann method (RLBM), and consider the influence of longitudinal length of sinus of Valsalva on blood flow fields around the aortic valves. As a result, we found that the longitudinal length of the sinus affects development of vortices around the aortic valves strongly. We also assessed the wall shear stress (WSS) distribution on the aortic valves and sinus wall and showed the effect of vortices in the sinus of Valsalva on local WSS distribution.**

Keywords- Aortic Valves; Sinus of Valsalva; Vorticity; Wall Shear Stress; Virtual Flux Method; Regularized Lattice Boltzmann Method

I. INTRODUCTION

Transposition of the great arteries (TGA) is one of the most severe congenital heart diseases. Since the aorta arises from the right ventricle in TGA, blood in the systemic circulation is always rich in carbon dioxide and poor in oxygen. On the other hand, the pulmonary circulation in TGA is always full of blood with oxygen. The systemic and pulmonary circulations are completely separated in TGA. The arterial switch operation (ASO) is the procedure of preference for treatment of TGA. Although many reports have shown good results after ASO [1, 2, 3], some patients suffer from circulatory system problems such as neo-aortic root dilatation and neo-aortic valve regurgitation [4, 5], and supravalvar pulmonary stenosis [6] after ASO. Diameters of aortic annulus and sinus of Valsalva 20 years after ASO are significantly wider in comparison to a normal population of young adults, whereas ascending aorta diameters are well preserved in our population and are not significantly different to the values in a normal population, demonstrating that dilatation of the aortic root is due to a localized problem [7]. This localized dilatation of the aortic root is often explained by the structural vascular difference between normal great arteries and the neo-aorta after ASO [8].

Fluid dynamic forces against the arterial wall should be considered as well as the structural difference. The morphology of the aorta and aortic valves movement strongly affect the blood flow fields in the aorta, especially at the root of the aorta. In addition, the sinus of Valsalva, which lies at the aortic root, plays an important role for aortic valves behaviour [9]. Since the aortic and pulmonary roots generally remain in situ after ASO, i.e., the original pulmonary artery is connected to the left ventricle (LV), whereas the original aorta is connected to the right ventricle, the neo-aorta has no sinus of Valsalva after ASO. Moreover, there are some cases that the curvature of the neo-aortic root is extremely larger than that in a normal population due to ASO. The influence of these morphological changes on the blood flow field at the aortic root should be investigated in detail to consider cardiovascular problems after ASO.

In the past study, we performed numerical simulation of blood flows around aortic valves by lattice Boltzmann method [10, 11]. The method of lattice Boltzmann equation (LBM) is a simple kinetic-based approach for fluid flow computation. The LBM has advantages in its simple coding and its locality, which makes it intrinsically parallelizable [12], and has been applied to many general problems [13, 14, 15], and those relevant to blood flow simulation [16, 17, 18], as well. However, stability of the simulation by LBM is strictly dependent on its relaxation time, which leads to restriction of the Reynolds number. Since blood flow simulation in the aorta is accompanied by high Reynolds number, it is necessary to improve stability of LBE. Izham et al. [19] proposed regularized lattice Boltzmann method (RLBM), which is based on the observation of symmetric condition in Chapman-Enskog expansion by Latt & Chopard [20], and it has successfully achieved higher stability in numerical simulation at high Reynolds number. In this study, we apply the virtual flux method (VFM) [21], which is a tool to describe stationary or moving body shapes in a Cartesian grid, to the 2D aortic valves and reproduce the blood flow fields

DOI: 10.5963/LSMR0303002

around the aortic valves and the sinus of Valsalva by RLBM, and consider the influence of longitudinal length of sinus of Valsalva on blood flow fields around the aortic valves.

II. METHODS

A. Computational Models

Numerical simulation of blood flow in the aorta with valves and sinus of Valsalva is performed. Figure 1 shows the schematic view of the 2-dimensional axisymmetric simulation model used in this study. The longitudinal length L and diameter D are set to 200 mm and 20 mm. The valve leaflets are modeled as arcs of a circle with a radius of $D/\sqrt{2}$, and placed at 80 mm (= 4D) from the inlet. The shape of the sinus of Valsalva is approximated as a semi-ellipse. The longitudinal length a and depth b of the sinus of Valsalva are set to a = 30 mm and b = 15 mm for Case 1, and a = 40 mm and b = 15 mm for Case 2, respectively as summarized in Table 1. The arterial wall and valves are described by virtual flux method on Cartesian coordinate as described below.

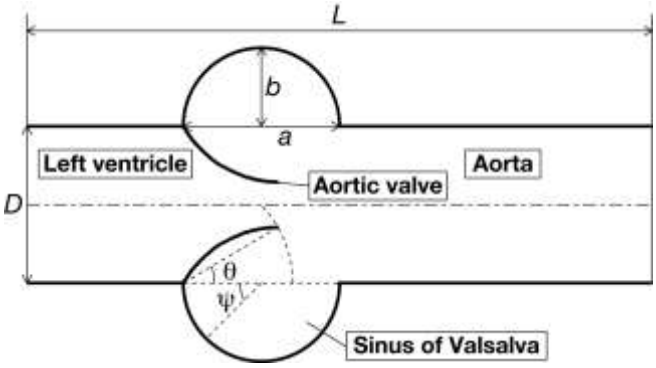

Figure 1 Schematic view of the computational model

TABLE I MORPHOROGY OF THE SINUS OF VALSALVA

	longitudinal length *a*	**depth *b***
case 1	30	15
case 2	40	15

B. Governing Equations

1) Lattice Boltzmann Method:

The discrete velocity Boltzmann equation (DVBE) is as follows,

$$\frac{\partial f_\alpha}{\partial t} + \boldsymbol{e}_\alpha \cdot \nabla f_\alpha = \boldsymbol{\Omega}_\alpha \tag{1}$$

where $\boldsymbol{e}_\alpha$ is the discrete particle velocity, f_α is the distribution function associated with $\boldsymbol{e}_\alpha$, and $\boldsymbol{\Omega}_\alpha$ is the collision operator. The collision operator, which is very complicated, is usually approximated by the simple single-relaxation-time Bhatnagar-Gross-Krook (BGK) model [22]:

$$\boldsymbol{\Omega}_\alpha = -\frac{1}{\tau}\left(f_\alpha - f_\alpha^{(eq)}\right) \tag{2}$$

where $f_\alpha{}^{(eq)}$ is the equilibrium distribution function, and τ is the relaxation time. The evolution of the distribution function f_α for the lattice Boltzmann equation can be written as

$$f_\alpha(\boldsymbol{x}+\boldsymbol{e}_\alpha\Delta t, t+\Delta t) - f_\alpha(\boldsymbol{x},t) = -\frac{1}{\tau}\left\{f_\alpha(\boldsymbol{x},t) - f_\alpha^{(eq)}(\boldsymbol{x},t)\right\} \tag{3}$$

In this study, we use a 2D square lattice model with 9 velocities, which is referred to as the D2Q9 model. It is shown that the Navier-Stokes equations can be derived from the LBM though a Chapman-Enskog expansion procedure in the incompressible limit [23] with a relaxation time τ as

$$\tau = \frac{3\nu}{c\delta x} + \frac{\delta t}{2} \tag{4}$$

DOI: 10.5963/LSMR0303002

The most common choice for the equilibrium distribution function $f_\alpha^{(eq)}$ is the truncated form of the Maxwell distribution, which is a very good approximation for small Mach numbers [24].

$$f_\alpha^{(eq)} = \omega_\alpha \rho \left[1 + \frac{3(\boldsymbol{e}_\alpha \cdot \boldsymbol{u})}{c^2} + \frac{9(\boldsymbol{e}_\alpha \cdot \boldsymbol{u})^2}{2c^4} - \frac{3\boldsymbol{u}^2}{2c^2} \right] \tag{5}$$

where ω_α is the weight coefficients.

2) Regularized Lattice Boltzmann Method:

The single-relaxation-time (SRT) LBM has been widely used for its simplicity, efficiency and ease of parallel programming implementation, however, it requires relatively large number of grids to simulate flows at even moderately high Reynolds number. In Chapman-Enskog expansion procedure, the non-equilibrium part of first-order is symmetrical with respect to spatial reflection. Latt & Chopard [20] observed that this symmetric condition is not necessarily satisfied and appears to take a non-negligible value in numerical simulations using SRT-LBM. Based on this observation, they considered a regularization step that enforces symmetrical property and proposed regularized lattice Boltzmann method (RLBM).

The relationships between stress tensor and distribution function in RLBM [19] is defined as

$$\Pi_{ij} = \sum_\alpha e_{\alpha i} e_{\alpha j} f_\alpha \tag{6}$$

where Π_{ij} is the stress tensor. The non-equilibrium part of the distribution and stress tensor were given as

$$f_\alpha^{(neq)} = f_\alpha - f_\alpha^{(eq)} \tag{7}$$

$$\Pi_{ij}^{(neq)} = \Pi_{ij} - \Pi_{ij}^{(eq)} \tag{8}$$

From the Chapman-Enskog expansion, the non-equilibrium part of ε-order can be explicitly derived as below,

$$f_\alpha^{(neq)} \approx f_\alpha^1 = -\frac{\delta t}{c_s^2} \tau \omega_\alpha \mathbf{Q}_{\alpha ij} \partial_i \rho u_j \tag{9}$$

$$\Pi_{ij}^{(neq)} \approx \sum_\alpha e_{\alpha i} e_{\alpha j} f_\alpha^1 = -\delta t c_s^2 \tau \left(\partial_i \rho u_j + \partial_j \rho u_i \right) \tag{10}$$

where $\mathbf{Q}_{\alpha ij}$ is defined as

$$\mathbf{Q}_{\alpha ij} = e_{\alpha i} e_{\alpha j} - c_s^2 \delta_{ij} \tag{11}$$

where c_s is the sound speed, and f_α^1 is then written as

$$f_\alpha^1 = \frac{\omega_\alpha}{2c_s^4} \mathbf{Q}_{\alpha ij} \Pi_{ij}^{(neq)} \tag{12}$$

By enforcing $f_\alpha^{(neq)} = f_\alpha^1$, the final form of the relaxation process can be written as

$$f_\alpha = f_\alpha^{(eq)} + \left(1 - \frac{1}{\tau} \right) f_\alpha^1 \tag{13}$$

The viscous stress tensor τ_{ij} can be evaluated using the non-equilibrium part of the distribution function [25] as

$$\tau_{ij} = \left(1 - \frac{1}{2\tau} \right) \sum_\alpha f_\alpha^{(neq)}(\boldsymbol{x}, t) \left(e_{\alpha i} e_{\alpha j} - \frac{1}{D} \boldsymbol{e}_\alpha \cdot \boldsymbol{e}_\alpha \delta_{ij} \right) \tag{14}$$

3) Aortic Valve Movement:

The aortic valves are assumed to be rigid, and their motion obeys following rigid-body rotation

$$\boldsymbol{T} = I \frac{d\boldsymbol{\omega}}{dt} \tag{15}$$

where $\boldsymbol{T}$ is the torque, I is the inertia moment, and ω is the angular velocity of the valve. The torque $\boldsymbol{T}$ is evaluated by force differences between LV-facing and aortic-facing surfaces of the valve,

$$\boldsymbol{T} = \sum \left(\boldsymbol{f}^{\mathrm{Ao}} - \boldsymbol{f}^{\mathrm{LV}} \right) \cdot r \tag{16}$$

DOI: 10.5963/LSMR0303002

where r is the radius of rotation. The forces acting on the valve are obtained by pressure p and viscous stress τ_{ii} as follows,

$$\boldsymbol{f} = (p + \tau_{ii}) \cdot dr \tag{17}$$

The inertia moment of the valve I is estimated by assuming the density of the valve is equal to that of the blood. The angular velocity ω is obtained by first-order Euler method.

$$\boldsymbol{\omega}(t + \Delta t) = \boldsymbol{\omega}(t) + \Delta t \frac{\boldsymbol{T}(t)}{I} \tag{18}$$

C. Boundary Conditions

The virtual flux method (VFM) enables us to estimate flow field around arbitrary body shapes properly in a Cartesian grid [21]. In this study, we apply the VFM to express arbitrary body shapes appropriately in case that boundary points are not located on the cell vertex. Figure 2 shows an example of virtual flux boundary, where the virtual boundary point b is placed between cell vertexes 1 and 3. When the distribution function at vertex 1 is obtained, the distribution function at vertex 3, which includes the effect of the virtual boundary, is necessary, and vice versa. The macroscopic quantities on the virtual boundary point b are then determined to satisfy the boundary conditions. No-slip condition on the boundary, for example, is attained to assume zero pressure gradient and zero velocity on the boundary.

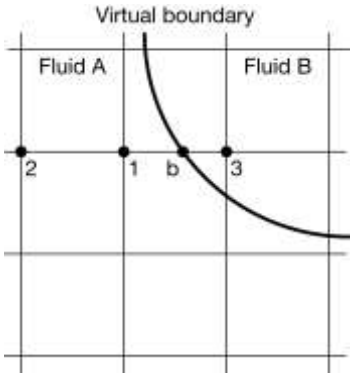

Figure 2 Schematic view of the virtual boundary in a Cartesian grid
The virtual boundary separates Fluid A from Fluid B completely.

Next, the equilibrium distribution function $f_\alpha^{(eq)}$ and distribution function f_α at the virtual boundary point b are obtained from the macroscopic quantities there. The distribution function f_α at the vertex 3 is then estimated to extrapolate that at the virtual boundary point b.

Axial velocity u at the inlet and pressure p at the outlet are given as shown in Fig. 3, which are modeled as blood flow from left ventricle and aortic pressure, respectively. Other parameters are linearly extrapolated. No-slip conditions are assumed on the wall and aortic valves. The Reynolds number Re at the peak velocity in Fig. 3 corresponds to 2,000. The period of the cycle is set to 1.0 s, and totally eight cardiac cycles, including three pre-cycles as preparation, are conducted for the blood flow simulation.

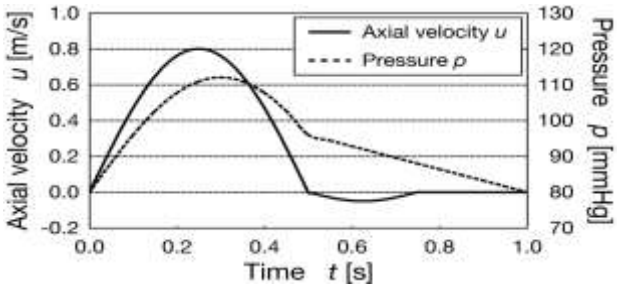

Figure 3 Axial velocity at the inlet and pressure at the outlet
The Reynolds number Re at the peak velocity corresponds to 2,000. The period of the cardiac cycle is set to 1.0 s.

III. RESULTS

Figure 4 shows the vorticity distribution and velocity vectors on the left for Case 1 and right for Case 2 in the seventh cardiac cycle at the time interval of 0.1 s. When the pressure at the LV exceeds that at the aorta, the valves start to open and blood flows toward the aorta passing through the aortic orifice. Vortices evolved from the tip of the valve spread and strike on the distal edge of the sinus of Valsalva, then they are divided into multiple. These vortical motions then lead blood flow fields

DOI: 10.5963/LSMR0303002

in the aorta to be more complicated. The vortices for Case 2 are more developed and dominant near the distal edge of the sinus. The valves start closing motion and seal the aortic orifice when the blood flow from the LV stops. Since multiple vortices still remain within the sinus of Valsalva in diastole, the aortic valve movements in systole have minor differences from cycle to cycle due to these vortices.

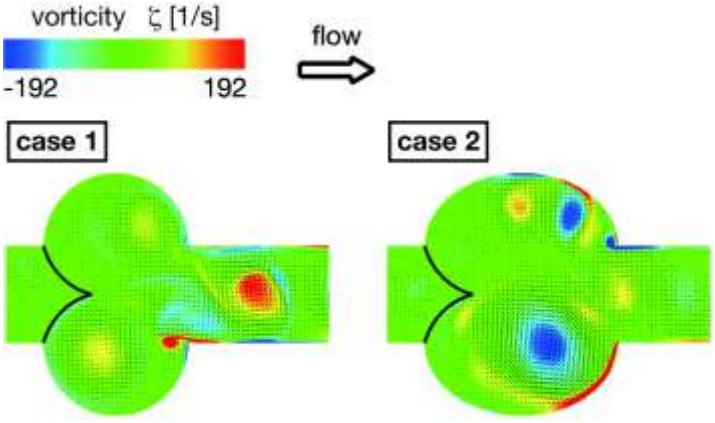

t = 0.0 [s]

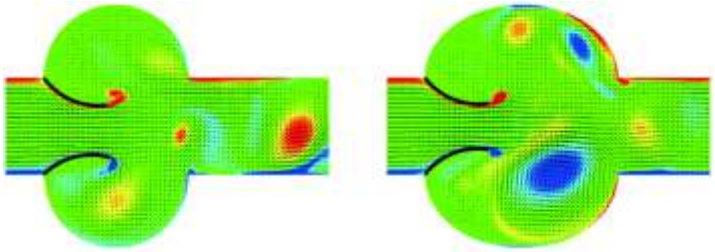

t = 0.1 [s]

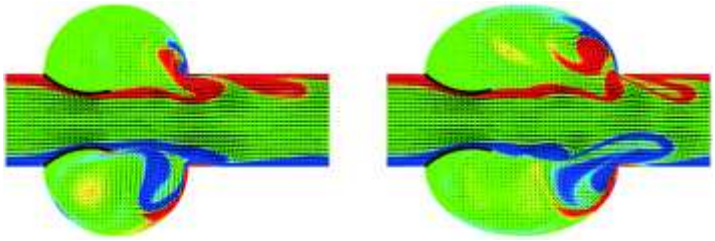

t = 0.2 [s]

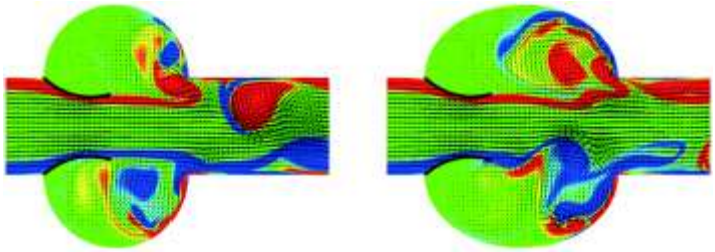

t = 0.3 [s]

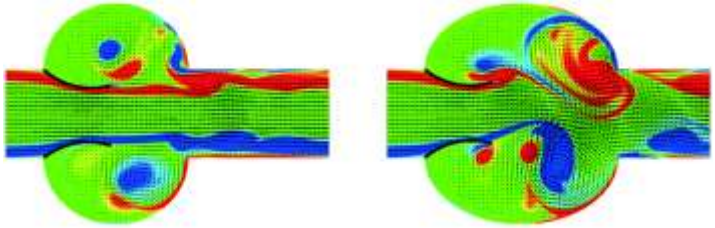

t = 0.4 [s]

DOI: 10.5963/LSMR0303002

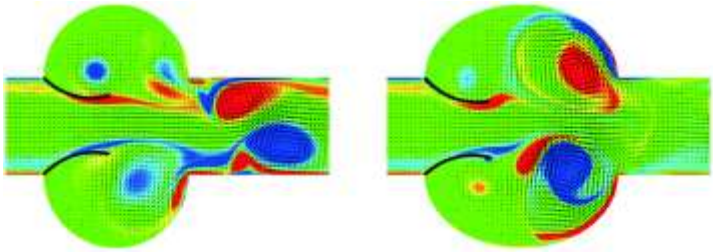

t = 0.5 [s]

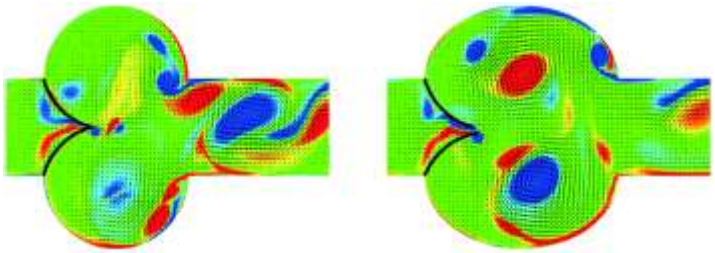

t = 0.6 [s]

Figure 4 Vorticity distribution and velocity vectors on the left for case 1 and right for case 2 in the seventh cardiac cycle at the time interval of 0.1 s

Figure 5 shows the averaged aortic valve movements in five cardiac cycles, i.e., from forth to eighth cardiac cycles in this study. The abscissa of the Fig. 5 is expressed by the time t of 0.0 to 1.0 for simplicity. The bold and thin lines denote Cases 1 and 2, respectively. The valve angle θ is defined as shown in Fig. 1, and θ of $\pi/4$ corresponds to the closed position. The aortic valves open immediately after blood ejects from the left ventricle in systole, and are closed around at t = 0.6 s. There are no significant differences between Cases 1 and 2 in terms of opening and closing valve timing, and the maximal aortic valve area, i.e., the minimal valve angle θ.

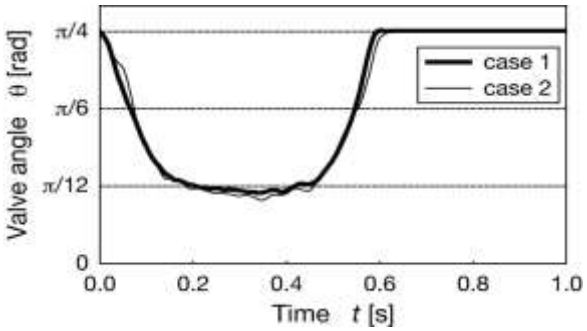

Figure 5 Averaged aortic valve movements in cardiac cycles

Figures 6 and 7 show the time averaged wall shear stress (WSS) diagrams on the LV-facing surface (Fig. 6) and aortic-facing surface (Fig. 7) of the aortic valve, which are important to discuss progression of cardiovascular disease such as atherosclerosis or aortic valve stenosis (see discussion below for details). These data are averaged in five cardiac cycles. In Fig. 6, the WSS reaches around 25 Pa at the center of the valve position owing to vena contracta, which is physiologically high. On the other hand, the WSS distribution on the aortic-facing surface is relatively flat, except for the tip of the valve (Fig. 7). The WSS distribution has no significant differences between Cases 1 and 2, except for the tip of the valve on the aortic-facing surface.

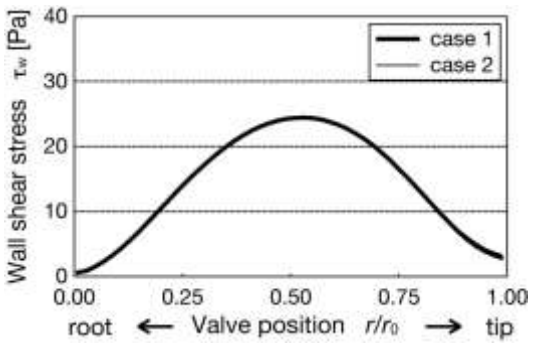

Figure 6 Time averaged WSS distribution on the LV-facing surface

DOI: 10.5963/LSMR0303002

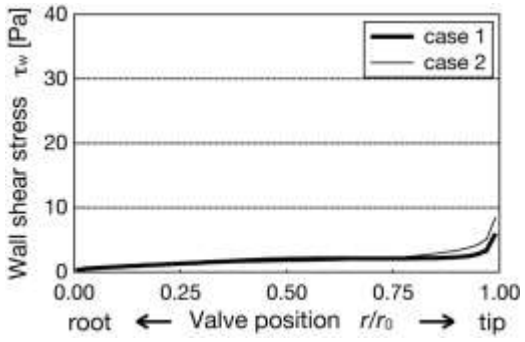

Figure 7 Time averaged WSS distribution on the aortic-facing surface

Figure 8 shows the time averaged WSS distribution on the sinus wall in five cardiac cycles. The sinus position $\psi = 0$ and π rad correspond to proximal and distal edges of the sinus of Valsalva, respectively as shown in Fig. 1. The WSS value in the range of $\psi = 0$ to $2\pi/3$ is around 1.0 Pa. Then it increases to 5.0 Pa and more toward the distal edge of the sinus. The WSS difference between Cases 1 and 2 is more remarkable toward the distally, especially after the sinus position ψ of $2\pi/3$. The WSS value for Case 2 is twice as large as that for Case 1 toward the distal edge.

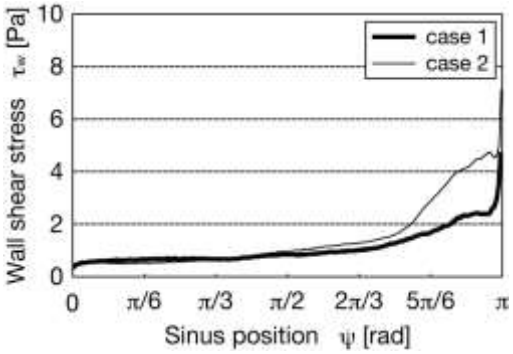

Figure 8 Time averaged WSS distribution on the sinus wall
The sinus position $\psi = 0$ and π rad correspond to proximal and distal edges of the sinus of Valsalva, respectively.

IV. DISCUSSION

The heart pumps blood throughout the body efficiently owing to the heart valves operation. When blood ejects from the LV, vortices are observed within the sinus of Valsalva as shown in Fig. 4 (t = 0.3 ~ 0.4 s). This vortical motion has the advantage of preventing the valve leaflet from bulging outward to contact the walls of the sinuses. The vortices for Case 2 are more dominant near the distal edge of the sinus, indicating that there needs an appropriate longitudinal length of the sinus for vortex development. The open sinus chamber thus can be supplied with fluid to fill the increasing volume behind the valve leaflets as they move toward closure (t = 0.5 ~ 0.6 s). After the valves close the aortic orifice, multiple vortices do not completely dissipate in the aorta as well as in the sinus of Valsalva in diastole, so that they persist until the next systole.

The valve movements are almost the same between Cases 1 and 2 as shown in Fig. 5, though vortices within the sinus of Valsalva are totally different. Bellhouse & Talbot [26] considered the important function of the sinus in aortic valves operation, and suggested that the trapped vortex within the sinus interacts with the decelerating flow field and thus pushes the leaflets into the aorta. According to their observation, the ratio of the total reversed flow to the forward flow in the absence of the sinuses is about 25%. To study the role of the sinus of Valsalva in valve closure at the physiological value of the Strouhal number, van Steenhoven & van Dongen [27] assessed the influence of the shape of the sinus on valve closure. They showed the presence of a cavity of a certain minimum size is essential in both longitudinal and radial directions for the mechanism of valve closure in the deceleration phase of systole. A larger ratio of sinus radius to leaflet length than the physiological one appears to result in a faster closure. There also exist some papers related to sinus of Valsalva, which suggest the importance of role in minimizing stresses in the valve leaflets [28, 29]. Relationships between size of sinus of Valsalva and aortic valves operation should be more investigated from the viewpoint of fluid dynamics.

Clinically, aortic valve stenosis (AS) is regarded as one of the most common diseases related to dysfunction of the heart valves. The opening area of the valve decreases due to AS, which cause considerable reduction of amount of blood flow. Classically, patients develop the 3 “S” rule of AS: Shortness of breath, Syncope, and Sudden death [30]. The mechanism of AS development remains unclear, yet mechanical forces are believed to be responsible for the morphologic change in the valve apparatus [31]. Thickening of the valve leaflets on the aortic-facing surface seems to be composed of plaquelike lesions. Accumulated within these lesions are proinflammatory and inflammatory components similar to those seen in atherosclerotic lesions. It is well known that the WSS plays a dominant role in determining the physiological mechanisms of the endothelial

DOI: 10.5963/LSMR0303002

cell in all generations of arteries, and developing vascular pathology such as atherosclerosis [32, 33, 34]. According to Malek et al. [35], the value of the low shear stress that causes atherosclerosis initiation is 0.4 Pa. Statistically significant inverse relationships between intima-media thickness and local WSS have also been reported [36, 37]. It is, therefore, important to investigate the WSS distribution in time and space in order to predict the precise region where AS occurs. Especially, since histopathology of the AS is similar to atherosclerosis, localized low shear stress region, i.e., the value of under 0.4 Pa, could be a candidate for AS initiation.

The WSS distribution of the aortic valves in cardiac cycle was higher on the LV-facing surface. The highest WSS region is the center of the valve position as shown in Fig. 6. This is mainly due to vena contracta at the narrowest aortic orifice. The aortic valves in this study were modeled as rigid arcs, whose movements were assumed to be rigid-body rotation. Owing to these assumptions, the valves behaviour is accompanied with no deflection or bending. Physiologically high WSS values, i.e., 10 Pa and more, on the LV-facing surface are attributed to these simplified heart valves model in this study. Improvement of the heart valves modeling should be considered in the future work.

The vortices evolved from the tip of the valve strike on the distal edge of the sinus and spread within the sinus of Valsalva. These vortices affect the WSS distribution of the valves on the tip of the aortic-facing surface and sinus wall near the distal edge. Especially, since the WSS values for Case 2 are higher than that for Case 1, the WSS distribution is strongly influenced by the vortex development around the aortic valves. On the other hand, the WSS distribution at the root of the valve on the aortic-facing surface is less influenced by the vortical motion, and the value always remains under 1.0 Pa. The WSS value is not low enough for initiation of AS as mentioned above, however, this region could be considered as one of the AS initiation areas based on the low shear stress hypothesis. More researches are necessary for better understanding on AS progression. Our computational scheme is suitable and promising to reproduce heart valves behavior with neither re-mesh nor re-construction of the model. Incorporating effect of deflection or bending of the heart valves behavior to our computational model will enable us to consider more accurate WSS distribution on the aortic valves and AS growth as well.

V. CONCLUSIONS

In this paper, we assessed the WSS distribution on the aortic valves and sinus wall and showed the effect of vortices in the sinus of Valsalva on local WSS distribution. The longitudinal length of the sinus affects development of vortices around the aortic valves strongly. In future work, more accurate researches are necessary to consider growth of cardiovascular disease such as atherosclerosis or aortic valve stenosis.

REFERENCES

[1] C. Planche, J. Bruniaux, F. Lacour-Gayet, J. Kachaner, J. P. Binet, D. Sidi, and E. Villain, “Switch operation for transposition of the great arteries in neonates. A study of 120 patients,” Journal of Thoracic Cardiovascular Surgery, vol. 96, pp. 354-363, 1988.

[2] R. Pretre, D. Tamisier, P. Bonhoeffer, P. Mauriat, P. Pouard, D. Sidi, and P. Vouhe, “Results of the arterial switch operation in neonates with transposed great arteries,” Lancet, vol. 357, pp. 1826-1830, 2001.

[3] W. G. Williams, B. W. McCrindle, D. A. Ashburn, R. A. Jonas, C. Mavroudis, and E. H. Black-stone, “Outcomes of 829 neonates with complete transposition of the great arteries 12-17 years after repair,” European Journal of Cardio-thoracic Surgery, vol. 24, pp. 1-10, 2003.

[4] C. J. McMahon, W. J. Ravekes, E. O. Smith, S. W. Denfield, R. H. Pignatelli, C. A. Altman, and N. A. Ayres, “Risk factors for neo-aortic root enlargement and aortic regurgitation following arterial switch operation,” Pediatric Cardiology, vol. 25, pp. 329-335, 2004.

[5] J. Losay, A. Touchot, A. Capderou, J. D. Piot, E. Belli, C. Planche, and A. Serraf, “Aortic valve regurgitation after arterial switch operation for transposition of the great arteries: Incidence, Risk factors, and Outcome,” Journal of the American College of Cardiology, vol. 47, pp. 2057-2062, 2006.

[6] M. F. Swartz, A. Sena, N. Atallah-Yunes, C. Meagher, J. M. Cholette, F. Gensini, and G. M. Alfieris, “Decreased incidence of supravalvar pulmonary stenosis after arterial switch operation,” Circulation, vol. 126, pp. S118-S122, 2012.

[7] K. D. H. M. Vandekerckhove, N. A. Blom, S. Lalezari, D. R. Koolbergen, M. E. B. Rijlaarsdam, M. G. Hazekamp, “Long-term follow-up of arterial switch operation with an emphasis on function and dimensions of left ventricle and aorta,” European Journal of Cardio-thoracic Surgery, vol. 35, pp. 582-588, 2009.

[8] S. Lalezari, M. G. Hazekamp, M. M. Bartelings, P. H. Schoof, and A. C. Gittenberger-De Groot, “Pulmonary artery remodeling in transposition of the great arteries: relevance for neoaortic root dilatation,” Journal of Thoracic Cardiovascular Surgery, vol. 126, pp. 1053-1060, 2003.

[9] Y. C. Fung, Biomechanics Circulation, 2nd edition, New York Berlin Heidelbelg: Springer-Verlag, pp. 42-48, 1997.

[10] T. Fukui and K. Morinishi, “Aortic valve oscillation due to vortices in the sinus of Valsalva by virtual flux method,” in Proceedings of the 8th KSME-JSME Thermal and Fluids Engineering Conference, 2012, pp. 1-4.

[11] T. Fukui and K. Morinishi, “Numerical simulation of blood flows in the aorta with aortic valves by virtual flux method,” in Proceedings of the European Congress on Computational Methods in Applied Sciences and Engineering, 2012, pp. 1-10.

[12] T. Kruger, F. Varnik, and D. Raabe, “Shear stress in lattice Boltzmann simulations,” Physical Review E, vol. 79(046704), pp. 1-14, 2009.

[13] D. Yu, R. Mei, L. S. Luo and W. Shyy, “Viscous flow computations with the method of lattice Boltzmann equation,” Progress in Aerospace Science, vol. 39, pp. 329-367, 2003.

DOI: 10.5963/LSMR0303002

[14] J. Zhang, G. Yan, and X. Shi, "Lattice Boltzmann model for wave propagation," Physical Review E, vol. 80(026706), pp. 1-13, 2009.

[15] J. C. G. Verschaeve, "Analysis of the lattice Boltzmann Bhatnagar-Gross-Krook no-slip boundary condition: Ways to improve accuracy and stability," Physical Review E, vol. 80(036703), pp. 1-23, 2009.

[16] J. Boyd, J. Buick, J. A. Cosgrove, and P. Stansell, "Application of the lattice Boltzmann model to simulated stenosis growth in a two-dimensional carotid artery," Physics in Medicine and Biology, vol. 50, pp. 4783-4796, 2005.

[17] M. Tamagawa, H. Kaneda, M. Hiramoto, and S. Nagahama, "Simulation of thrombus formation in shear flows using lattice Boltzmann method," Artificial Organs, vol. 33(8), pp. 604-610, 2009.

[18] L. Axner, A. G. Hoekstra, A. Jeays, P. Lawford, R. Hose, and P. M. A. Sloot, "Simulations of time harmonic blood flow in the Mesenteric artery: comparing finite element and lattice Boltzmann methods," Biomedical Engineering Online, vol. 8(23), pp. 1-8, 2009.

[19] M. Izham, T. Fukui, and K. Morinishi, "Application of regularized lattice Boltzmann method for incompressible flow simulation at high Reynolds number and flow with curved boundary," Journal of Fluid Science and Technology, vol. 6(6), pp. 812-821, 2011.

[20] J. Latt and B. Chopard, "Lattice Boltzmann method with regularized precollision distribution functions," Mathematics and Computers in Simulation, vol. 72, pp. 165-168, 2006.

[21] I. Tanno, K. Morinishi, K. Matsuno, and H. Nishida, "Validation of virtual flux method for forced convection flow," JSME International Journal, vol. B49(4), pp. 1141-1148, 2006.

[22] P. L. Bhatnagar, E. P. Gross, and M. Krook, "A model for collision processes in gases: I. Small amplitude processes in changed and neutral one-component system," Physical Review, vol. 94, pp. 511-525, 1954.

[23] J. D. Sterling and S. Chen, "Stability analysis of lattice Boltzmann methods," Journal of Computational Physics, vol. 123, pp. 196-206, 1996.

[24] Y. H. Quian, D. d'Humieres, and P. Lallemand, "Lattice BGK models for Navier-Stokes equation," Europhysics Letters, vol. 17, pp. 479-484, 1992.

[25] R. Mei, D. Yu, and W. Shyy, "Force evaluation in the lattice Boltzmann method involving curved geometry," Physical Review E, vol. 65(041203), pp. 1-14, 2002.

[26] B. J. Bellhouse and L. Talbot, "The fluid mechanics of the aortic valve," Journal of Fluid Mechanics, vol. 35, pp. 721-735, 1969.

[27] A. A. van Steenhoven and M. E. H. van Dongen, "Model studies of the closing behavior of the aortic valve," Journal of Fluid Mechanics, vol. 90, pp. 21-32, 1979.

[28] M. J. Thubrikar, S. P. Nolan, J. Aouad, and J. D. Deck, "Stress-sharing between the sinus and leaflets of canine aortic valve," Annals of Thoracic Surgery, vol. 42, pp. 434-440, 1986.

[29] A. Beck, M. J. Thubrikar, and F. Robicsek, "Stress analysis of the aortic valve with and without the sinuses of Valsalva," Journal of Heart Valve Disease, vol. 10, pp. 1-11, 2001.

[30] C. Z. Zigelman and P. M. Edelstein, "Aortic valve stenosis," Anesthesiology clinics, vol. 27, pp. 519-532, 2009.

[31] R. V. Freeman and C. M. Otto, "Spectrum of calcific aortic valve disease: pathogenesis, disease progression and treatment strategies," Circulation, vol. 111, pp. 3316-3326, 2005.

[32] C. G. Caro, J. M. Fitzgerald, and R. C. Schroter, "Atheroma and arterial wall shear: observation, correlation and proposal of a shear dependent mass transfer mechanism for atherogenesis," Proceedings of the Royal Society, vol. 177, pp. 109-159, 1971.

[33] D. L. Fry, "Certain histological and chemical responses of the vascular interface to acutely induced mechanical stress in the aorta of the dog," Circulation Research, vol. 24, pp. 93-108, 1969.

[34] D. P. Giddens, C. K. Zarins, and S. Glagov, "The role of fluid mechanics in the localization and detection of atherosclerosis," Journal of Biomechanical Engineering, vol. 115, pp. 588-594, 1993.

[35] A. M. Malek, A. L. Alper, and S. Izumo, "Hemodynamic shear stress and its role in atherosclerosis," Journal of the American Medical Association, vol. 282, pp. 2035-2042, 1999.

[36] A. Gnasso, C. Carallo, C. Irace, V. Spagnuolo, G. De Novara, P. L. Mattioli, and A. Pujia, "Association between intima-media thickness and wall shear stress in common carotid arteries in healthy male subjects," Circulation, vol. 94, pp. 3257-3262, 1996.

[37] C. Irac, C. Cortese, E. Fiaschi, C. Carallo, E. Farinaro, and A. Gnasso, "Wall shear stress is associated with intima-media thickness and carotid atherosclerosis in subjects at low coronary heart disease risk," Stroke, vol. 35, pp. 464-468, 2004.

DOI: 10.5963/LSMR0303002